Plasma-enhanced Low-temperature Solid-state Synthesis of Spinel LiMn2O4 with Superior Performance for Lithium Ion Batteries

Journal:	*Green Chemistry*
Manuscript ID:	GC-COM-07-2015-001563.R2
Article Type:	Communication
Date Submitted by the Author:	21-Aug-2015
Complete List of Authors:	Jiang, Qianqian; Shenzhen University, College of Photoelectric engineering Ma, Zhaoling; Hunan University, Zhang, Han; Shenzhen University, Wang, Shuangyin; Hunan University,

Green Chemistry RSCPublishing

COMMUNICATION

Plasma-enhanced Low-temperature Solid-state Synthesis of Spinel $LiMn_2O_4$ with Superior Performance for Lithium-ion Batteries

Cite this: DOI: 10.1039/x0xx00000x

Qianqian Jiang[a], Zhaoling Ma[b], Han Zhang[*, a] and Shuangyin Wang[*, b]

Received 00th January 2012,
Accepted 00th January 2012

DOI: 10.1039/x0xx00000x

www.rsc.org/

Abstract

The spinel $LiMn_2O_4$, for the first time, is synthesized a novel plasma-enhanced low-temperature solid-state approach strategy. The $LiMn_2O_4$ shows superior performance with higher capacity and significantly improved cycling stability. The plasma-enhanced strategy offers a new technique for efficient synthesis of electrode materials for batteries.

1. Introduction

Lithium-ion batteries have been used in electric vehicles, portable power tools, medical equipment and hybrid electric vehicles [1-4] due to their high energy densities. Lithium manganese oxide ($LiMn_2O_4$) with a spinel structure possessing characteristics of abundant resources, low cost, environmental friendship, safety, high voltage, and high-capacity is one of the most widely used cathode materials in lithium rechargeable batteries, which has been a hot research topic in the field of lithium-ion batteries.[5-7] A variety of techniques have been developed for the preparation of $LiMn_2O_4$, including RF sputtering (radio frequency), hydrothermal chemical synthesis, flame spray pyrolysis, solid-state thermal annealing etc. Among these techniques, the solid-state thermal annealing method is one of most extensively developed and used for the commercial synthesis of $LiMn_2O_4$,[8, 9] but it requires prolonged heat treatment at relatively high temperatures (> 750 °C) with repeatedly intermediate grinding.[10-12] Moreover, this method also has many disadvantages such as poor control over the crystalline growth, in-homogeneity, irregular morphology, large particle size, broad particle size distribution and so on. [13-18] Since the solid-state method is more ready for large-scale commercialization of $LiMn_2O_4$ but consumes much energy during its preparation, it's of essential importance to develop novel low-temperature and fast solid-state strategy to reduce the energy consumption for the preparation of $LiMn_2O_4$. From the chemistry viewpoint, in order to reduce the energy consumption, that is, to lower the reaction temperature and time, the reaction kinetics of the synthesis of $LiMn_2O_4$ must be significantly enhanced at a relatively low temperature and shorten reaction time.

Plasma as one of the four fundamental states of matter, the others being solid, liquid and gas, has very different properties from the other states. Plasma consists of charged particles (such as positive ions, negative ions, electrons, free radicals and reactive species) and a set of neutral particles. In plasma, the positive and

a SZU-NUS Collaborative Innovation Center for Optoelectronic Science and Technology, Key Laboratory of Optoelectronic Devices and Systems of Ministry of Education and Guangdong Province, College of Optoelectronic Engineering, Shenzhen University, Shenzhen 518060, China
b State Key Laboratory of Chem/Bio-Sensing and Chemometrics, College of Chemistry and Chemical Engineering, Hunan University Changsha, 410082, P. R. China
E-mail: hzhang@szu.edu.cn (H.Z.), shuangyinwang@hnu.edu.cn(S. W.)

negative ions are completely free showing a high chemical activity. Through the inelastic collision between each other, the activation state of reactant ion is formed, which can relatively easily promote the chemical reaction. Nowadays, the plasma has been applied into the synthesis of ammonia,[19] organic material,[20] carbon nanotubes[21, 22] and so on.[23] It has been demonstrated that the plasma-assisted method can efficiently promote the preparation of the target materials with good performance.

In this work, for the first time, we develop a plasma-enhanced low-temperature solid-state strategy to prepare $LiMn_2O_4$ with low energy consumption and superior performance for lithium-ion batteries. The as-prepared $LiMn_2O_4$ shows a narrow particle size distribution in the range of 400-450 nm and smaller mean particle size. The improved quality of the $LiMn_2O_4$ products leads to significantly enhanced electrochemical performance as the cathode materials in lithium-ion batteries. For the plasma-enhanced low-temperature solid-state synthesis of $LiMn_2O_4$, a plasma-enhanced tube furnace is used, as shown in Scheme 1, which mainly consists of a vacuum pump, a pressure probe, a tube furnace, a plasma generator, a condenser and a flow meter.

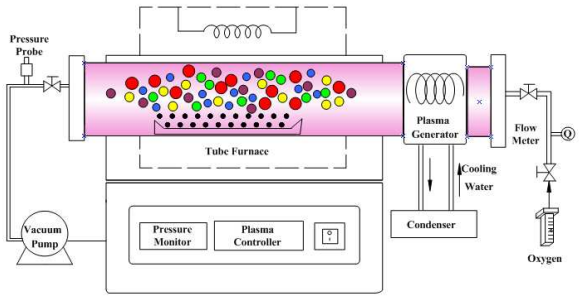

Scheme 1. Schematic diagram of the plasma-enhanced tube furnace for the preparation of $LiMn_2O_4$.

2. Experimental

Synthesis of chemical manganese dioxide (CMD) and $LiMn_2O_4$.

Lithium hydroxide selected as a lithium source and chemical manganese dioxide (CMD) as a manganese source with a stoichiometric molar ratio of 1:2 are mixed, then ball-milled for 2 h. CMD is prepared through a redox process using $KMnO_4$ and $MnCl_2{\cdot}4H_2O$ as reactants. Mn^{7+} in $KMnO_4$ is reduced, while Mn^{2+} is oxidized to Mn^{4+} in MnO_2 and no additional oxidants or reducing agents are added in this process. The mixture is introduced into the plasma-enhanced tube furnace. Plasma is generated by an radio frequency (RF) power supply at 13.56 MHz, and the applied RF power is set at 200 W and the temperature of the tube furnace is set at 500 °C. The flow rate of oxygen is set at 3 standard-state cubic centimeter per minute (sccm) and the total pressure in the chamber is kept at 66 Pa. The reaction takes about 30 mins. The spinel $LiMn_2O_4$ synthesized by the above process is referred as PLA-LMO-30. For comparison, the conventional spinel $LiMn_2O_4$ is also prepared by the conventional annealing method at 800 °C for 40 min and 4 h, and the resultant sample is referred to LMO-40 and LMO-4h, respectively.

Materials characterization.

X-ray diffraction studies are carried using on an X-ray diffractometer (D/MAX-2200V, Rigaku, Japan) with Cu-Kα radiation. The morphology and crystal lattice of the sample are characterized by the Transmission Electron Microscope (TEM) (100CX-II made by JEOL, Tokyo, Japan). The Scanning Electron Microscopy (SEM) images are applied to observe morphologies of the samples by scanning electron microscopy (Hitach S-4800, Japan).

Electrochemical characterization

The different $LiMn_2O_4$ electrodes as fabricated above are integrated into two-electrode CR2032-type coin cells for electrochemical measurements, where $LiMn_2O_4$ electrodes are used as working electrode with metallic lithium foil as counter electrode; electrolyte consists of 1.0 $mol{\cdot}L^{-1}$ $LiPF_6$ in ethylene carbonate (EC) and dimethyl carbonate (DMC) in a 1:1 (v/v) ratio. The cells are charged and discharged within the potential range of 3.0~4.5 V at the current density of 0.2 C (1 C=120 mA/g) using a LAND CT2001A battery tester (Wuhan, China) at room temperature. The electrochemical behaviors of $LiMn_2O_4$ are studied by cyclic voltammetry on

AUT85794 (made in the Netherland) with scan rate of 0.1 $mV \cdot s^{-1}$. And the electrochemical impedance spectroscopy (EIS) is measured on AUT85794 with the frequency range from 100 kHz and 10 mHz.

3. Results and discussion

X-ray diffraction patterns are collected to investigate the structural information of the as-prepared spinel $LiMn_2O_4$ by the plasma-enhanced low-temperature solid-state method (PLA-LMO-30) and the conventional thermal annealing method (LMO-4h), as shown in Figure 1. The diffraction peaks of the sample PLA-LMO-30 is clearly indexed to the spinel $LiMn_2O_4$, which confirms the successful formation of the spinel $LiMn_2O_4$. We also investigate the effect of the reaction time during the preparation of $LiMn_2O_4$ by the plasma-enhanced method (PLA-LMO-X, X represents the reaction time-mins). As shown by the XRD patterns of PLA-LMO-Xs in Figure S1, all of the samples show the characteristic diffraction peaks, indicating the efficiency of the plasma-enhanced strategy. For PLA-LMO-20, a small amount of MnO_2 signals are also detected, probably due to the incomplete conversion to the product within such a short time. For the sample LMO-4h prepared by the conventional thermal annealing method (800 ^oC, 4 h), the similar diffraction peaks are also observed, confirming the formation of the spinel $LiMn_2O_4$. By comparing the two samples (PLA-LMO-30 and LMO-4h), it can be found that the full width at half-maximum of the (111) and (311) lines of PLA-LMO-30 are larger than those of LMO-4h, which indicates that the plasma-enhanced strategy produced $LiMn_2O_4$ with smaller crystalline size. As a control, we also try to prepare $LiMn_2O_4$ by the conventional thermal annealing method for a shorter time (40 mins, which is still longer than the time for PLA-LMO-30, denoted as LMO-40). From the XRD patterns, it can be clearly seen that the diffraction peaks of the sample are indexed to the formation of MnO_2 but there is no $LiMn_2O_4$ signals although the sintering temperature is very high (800 ^oC). This control experiment demonstrated that short time (40 mins) is not enough for preparation of $LiMn_2O_4$ phase with the conventional thermal annealing method, but it works well with the plasma-enhanced method at even shorter time (30 mins). Therefore, the as-developed plasma-enhanced low-temperature solid-state method is of high efficiency for the preparation of $LiMn_2O_4$ electrode materials.

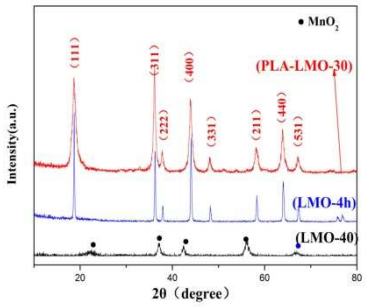

Figure 1. XRD patterns are collected to investigate the structural information of the as-prepared spinel $LiMn_2O_4$ by the plasma-enhanced low-temperature solid-state method (PLA-LMO-30) and the conventional thermal annealing method (LMO-40 and LMO-4h).

SEM images are collected to observe the surface morphology of PLA-LMO-30 and LMO-4h, as shown in Figure 2a-c. It can be clearly observed that the sample PLA-LMO-30 (Fig.2 a and b) shows the well-shaped polyhedral structure of spinel $LiMn_2O_4$ with the mean particle size of about 400 nm (Figure S3). In the case of the LMO-4h (Figure 2c), not only polyhedral but also few quasi-spherical can be observed with a larger particle size of about 500 nm. From the particle size distribution (Figure S3), we can find that the distribution of PLA-LMO-30 is better than LMO-4h, which is important for the electrochemical applications. The SEM characterizations successfully illustrates that the plasma-enhanced strategy can produce higher quality of $LiMn_2O_4$ with narrow size distribution and fine particles. With the plasma-enhanced strategy, different plasma irradiation time may lead to varying products. As shown by the SEM images of PLA-LMO with different plasma time (Figure S2), PLA-LMO-30 shows the best particle uniformity. With these physical properties, improved battery performance is expected using PLA-LMO-30 as the cathode materials. The transmission electron microscopy (TEM) images for $LiMn_2O_4$ prepared by the

plasma-enhanced method are shown in Figure S4. To get deep insight into the structural information, the high resolution TEM (HR-TEM) image is collected for PLA-LMO-30 as shown in Figure 2d. Figure 2d shows the atom arrangements of $LiMn_2O_4$ nano-particles, and the measured spacing of 0.48 nm can be indexed to the distance between (111) planes of $LiMn_2O_4$ [24].

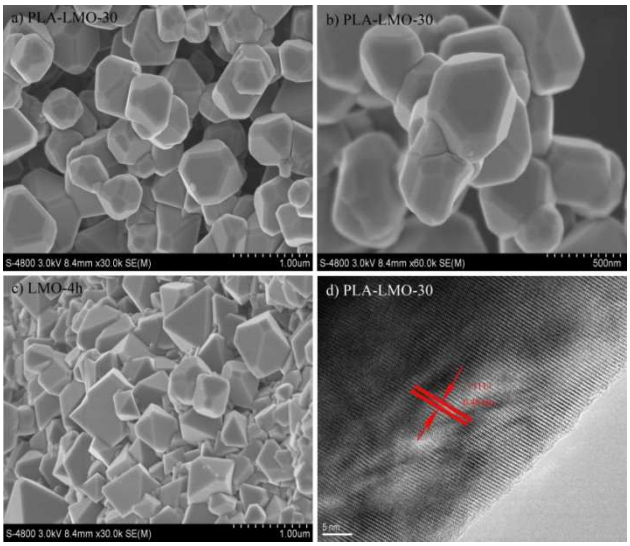

Figure 2. Some physical properties of the sample PLA-LMO-30 and LMO-4h: a, b) SEM images of PLA-LMO-30 show highly aggregated nano-particles. Scale bars: 1 μm (a), 500 nm (b); (c) SEM image of LMO-4h. Scale bar: 2 μm; (d) HR-TEM images of PLA-LMO-30.

The battery performance of the as-prepared samples PLA-LMO-30 and LMO-4h are shown in Figure 3. From the initial discharge curves (Figure 3a), we can clearly see that the initial discharge capacity of PLA-LMO-30 is 129.8 mAh/g which is higher than that of LMO-4h (114.8 mAh/g). On the other hand, PLA-LMO-20 and PLA-LMO-40 samples are also characterized in lithium-ion batteries (Figure S5). Compared with PLA-LMO-30, PLA-LMO-20 shows poorer performance, probably due to the incomplete reaction to obtain the pure spinel $LiMn_2O_4$ phase. With longer plasma reaction time to 30 mins, PLA-LMO-30 shows better discharge capacity. But with the further increase of the plasma time to 40 mins, the initial discharge becomes slightly lower than PLA-LMO-30 due to the increased average particle size (Figure S2), but it is still better than the LMO-4h prepared with the conventional method.

The cycling stability of the electrode materials is also a very important parameter for the use in batteries. Figure 3b shows the cycling properties of PLA-LMO-30 and LMO-4h. The discharge capacities of PLA-LMO-30 only decreased from 129.8 mAh/g to 123.9 mAh/g after 100 cycles with an average capacity loss of 0.059 mAh/g per cycle. In other words, after 100 charge/discharge cycles, the discharge capacity of PLA-LMO-30 can maintain 95.46% of its initial capacity. While the discharge capacities of LMO-4h decreased seriously from 114.8 mAh/g to 86.8 mAh/g after 100 cycles maintaining 75.61% of its initial capacity. It is obvious that the cycling performance of PLA-LMO-30 is superior to LMO-4h. More dramatically, PLA-LMO-30 almost shows the best battery performance by comparing with the reported $LiMn_2O_4$, as given in Table S1. These results clearly indicate that the $LiMn_2O_4$ obtained by the plasma-enhanced strategy can be used as a promising cathode material in lithium-ion batteries.

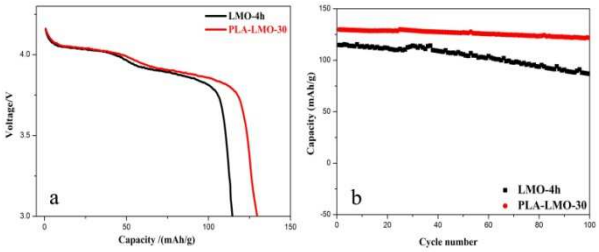

Figure 3. Electrochemical performance of the as-prepared samples PLA-LMO-30 and LMO-4h: (a) The Initial discharge curves (b) Discharge capacities vs. cycle number

The above battery testing demonstrated the high performance of $LiMn_2O_4$ prepared by the as-developed plasma-enhanced low-temperature solid-state strategy. Subsequently, cyclic voltammetry (CV) and electrochemical impedance spectroscopy (EIS) are carried out to investigate the electrochemical behaviors of electrode materials in batteries. The CV curves of PLA-LMO-30 and LMO-4h at a scan rate of 0.1 mV/s in the voltage range of 3.0~4.5 V (vs. Li/Li^+) are shown in Figure 4a. The corresponding data obtained

from Figure 4a are listed in Table S2 in details. Two couples of separate redox peaks (the anodic peak E_{O1} and E_{O2}, the cathodic peak E_{R1} and E_{R2}) are observed from CV curves of PLA-LMO-30 and LMO-4h, which corresponds to the de-intercalation and intercalation of Li^+ ions from/into the spinel host structure in the electrolyte.[25-27] In comparison with the CV curve of LMO-4h, the CV curve of PLA-LMO-30 shows two higher distinct oxidation current peaks at higher voltage, two high distinct reduction current peaks at lower voltage, indicating the occurrence of lower polarization and the reversible oxidation reaction process at the cathode, which further illustrates that the spinel $LiMn_2O_4$ synthesized by the plasma-enhanced method has the high electronic conductivity than the sample synthesized from the traditional solid state method.[28, 29] Furthermore, redox peaks of PLA-LMO-30 are larger and sharper than those of LMO-4h, which indicates that PLA-LMO-30 has larger capacity and faster electrode reaction than LMO-4h.[30] This cyclic voltammetric behavior is coincided with the initial discharge curves, indicating the sample PLA-LMO-30 shows better battery performance.

In order to further study the electrochemical behavior of $LiMn_2O_4$, electrochemical impedance spectroscopy before charge/discharge test with the two-electrode CR2032-type coin cells is recorded. Figure 4b shows the Nyquist plots for the two samples. The high frequency intercept at the Z' axis corresponds to the ohmic resistance (R_s), which represents the resistance of the electrolyte. The semicircle in the middle frequency range indicates the charge transfer resistance (R_{ct}).[31] The Warburg impedance (Z_w) relates to a combined effect of the diffusion of lithium ions on the electrode/electrolyte interfaces, which corresponds to the straight sloping line at low frequency end. [32] It can be seen that both cells have a similar ohmic resistance, but the semicircle of PLA-LMO-30 is much smaller than that of LMO-4h. From the fitted impedance parameters, the charge transfer resistance (R_{ct}) of the sample PLA-LMO-30 is smaller (R_{ct}≈71.6 Ω) than the sample LMO-4h (R_{ct}≈549.3 Ω), indicating the inserting and de-inserting of lithium-ions for PLA-LMO-30 are easier than for LMO-4h. In other words, the spinel $LiMn_2O_4$ synthesized by the plasma-enhanced solid state method with excellent electronic and ionic conductivities can greatly enhance rapid electron transport during the electrochemical lithium insertion/extraction reaction. The impedance results of PLA-LMO-30 and LMO-4h electrodes are consistent with the results from the other electrochemical measurements.[33] The as-observed advanced properties of PLA-LMO-30 over LMO-4h significantly contribute to its superior performance of PLA-LMO-30 based Li-ion battery in terms of high initial discharge capacity and excellent cycling stability.

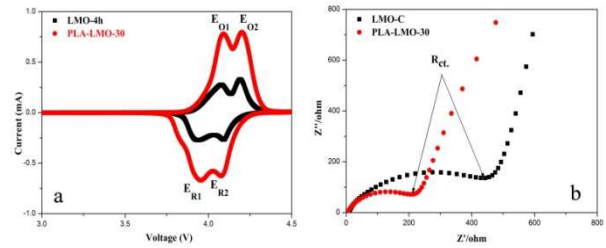

Figure 4. Cyclic voltammograms (a) and electrochemical impedance spectroscopy (b) of samples PLA-LMO-30 and LMO-4h.

Conclusions

A novel plasma-enhanced low-temperature solid-state strategy is developed to prepare spinel $LiMn_2O_4$ as cathode materials of rechargeable lithium-ion batteries. The as-prepared spinel $LiMn_2O_4$ shows superior performance for Li-ion battery in terms of initial discharge capacity and excellent cycling stability contributed by the fine particle size and narrow distribution with good electronic and ionic conductivity. More importantly, compared to the conventional high-temperature thermal annealing method, the plasma-enhanced low-temperature solid-state strategy is more efficient with much lower energy consumption. The as-developed strategy presents a new possibility to prepare cathode materials (even many other electrode materials including metal oxide etc.) with excellent electrochemical performances but with low energy consumption, which can accelerate the commercialization process of cathode material in lithium-ion battery.

Acknowledgements

The work is supported by the National Natural of Science Foundation of China (Grant No.: 51402100 and 61435010), the Youth 1000 Talent Program of China, Inter-discipline Research Program of Hunan University and China Postdoctoral Science Foundation Funded Project (No. 2014M552133).

Notes and references

1. B. Kang and G. Ceder, *Nature*, 2009, **458**, 190-193.
2. M. S. Whittingham, *Chem. Rev.*, 2004, **104**, 4271-4302.
3. H. Nishide, *Science*, 2008, **4**.
4. B. Deng, H. Nakamura and M. Yoshio, *J. Power Sources*, 2005, **141**, 116-121.
5. M. Armand and J. M. Tarascon, *Nature*, 2008, **451**, 652-657.
6. Q. Jiang, X. Wang, C. Miao and Z. Tang, *ermal method. RSC Adv.*, 2013, **3**, 12088.
7. H. Wu, J. Tu, Y. Yuan, X. Chen, J. Xiang, X. Zhao and G. Cao, *J. Power Sources*, 2006, **161**, 1260-1263.
8. J. Guan and M. Liu, *Solid State Ionics*, 1998, **110**, 21-28.
9. G. Li, A. Yamada, Y. Fukushima, K. Yamaura, T. Saito, T. Endo, H. Azuma, K. Sekai and Y. Nishi, *Solid State Ionics*, 2000, **130**, 221-228.
10. H. W. Chan, J. G. Duh and S. R. Sheen, J. Power Sources, 2003, **115**, 110-118.
11. J. M. Tarascon, E. Wang, F. Shokoohi, W. McKinnon and S. Colson, *J. Electrochem. Soc.*, 1991, **138**, 2859-2864.
12. X. Xiang, J. C. Knight, W. Li and A. Manthiram, *J. Phys. Chem. C*, 2014, **118**, 21826-21833.
13. M. Y. Song, D. S. Ahn and H. R. Park, *J. Power Sources*, 1999, **83**, 57-60.
14. K. Nishimura, T. Douzono, M. Kasai, H. Andou, Y. Muranaka and Y. Kozono, *J. Power Sources*, 1999, **81**, 420-424.
15. M. Okubo, D. Asakura, Y. Mizuno, J.-D. Kim, T. Mizokawa, T. Kudo and I. Honma, *J. Phys. Chem. Lett.*, 2010, **1**, 2063-2071.
16. M. Hirayama, H. Ido, K. Kim, W. Cho, K. Tamura, J. i. Mizuki and R. Kanno, *J. Am. Chem. Soc.*, 2010, **132**, 15268-15276.
17. Q. Jiang, X. Wang and Z. Tang, *Fuller. Nano. Tub. Car. N.*, 2014, **23**, 676-679.
18. S. H. Ye, J. K. Bo, C. Z. Li, J. S. Cao, Q. L. Sun and Y. L. Wang, *Electrochim. Acta*, 2010, **55**, 2972-2977.
19. G. Vissokov, *Journal of materials science*, 1998, **33**, 3711-3720.
20. Y. S. Lin and H. K. Yasuda, *J. Polym. Sci., Part B: Polym. Phys.*, 2003, **41**, 2004-2021.
21. G. P. Vissokov, *Catal. today*, 2004, **89**, 205-211.
22. G. P. Vissokov, *Catal. Today*, 2004, **89**, 223-231.
23. C.-j. Liu, G. P. Vissokov and B. W.-L. Jang, *Catal. Today*, 2002, **72**, 173-184.
24. M. Zhao, X. Song, F. Wang, W. Dai and X. Lu, *Electrochim. Acta*, 2011, **56**, 5673-5678.
25. X. Wang, Y. Hou, Y. Zhu, Y. Wu and R. Holze, *Sci. Rep.*, 2013, **3**.
26. K. Kanamura, H. Naito, T. Yao and Z.-i. Takehara, *J. Mater. Chem.*, 1996, **6**, 33-36.
27. W. Tang, S. Tian, L. Liu, L. Li, H. Zhang, Y. Yue, Y. Bai, Y. Wu and K. Zhu, *Electrochem. Commun.*, 2011, **13**, 205-208.
28. M. G. Kim, H. Kim and J. Cho, *J. Solid State Electrochem.*, 2010, **157**, A802-A807.
29. H. Ming, Y. Yan, J. Ming, J. Adkins, X. Li, Q. Zhou and J. Zheng, *Electrochim. Acta*, 2014, **120**, 390-397.
30. S. T. Yang, J. H. Jia, L. Ding and M. C. Zhang, *Electrochim.Acta*, 2003, **48**, 569-573.
31. M. Mohamedi, D. Takahashi, T. Uchiyama, T. Itoh, M. Nishizawa and I. Uchida, *J. Power Sources*, 2001, **93**, 93-103.
32. S. S. Zhang, K. Xu and T. R. Jow, *Electrochimica Acta*, 2006, **51**, 1636-1640.
33. D. Guo, Z. Chang, H. Tang, B. Li, X. Xu, X.-Z. Yuan and H. Wang, *Electrochim. Acta*, 2014, **123**, 254-259.

Electronic Supplementary Information (ESI) available: [details of any supplementary information available should be included here]. See DOI: 10.1039/c000000x/